Inorg. Chem. **2004**, *43*, 6061–6066

Synthesis of α-$MoTe_2$ Nanorods via Annealing Te-Seeded Amorphous $MoTe_2$ Particles

Longhui Qiu,[†,‡] Yun Wei,[‡] Vilas G. Pol,[†] and Aharon Gedanken*[,†]

Department of Chemistry, Bar-Ilan University, Ramat-Gan 52900, Israel, and Research Centre of Laser Fusion, China Academy of Engineering Physics, Mianyang 621900, China

Received March 28, 2004

Semiconductor α-$MoTe_2$ nanorods have been synthesized by annealing Te-seeded particles of an amorphous $MoTe_2$ intermediate. This intermediate is prepared by a solution reaction between $Mo(CO)_6$ and elemental Te in diphenylmethane. The as-synthesized products were characterized by structural, compositional, and morphological techniques of X-ray diffraction, selected area electron diffraction, selected area energy dispersive spectroscopy, energy dispersive X-ray analysis, X-ray photoelectron spectroscopy, transmission electron microscopy, and high-resolution transmission electron microscopy. The results of the annealing process are $MoTe_2$ nanorods with diameters of 50–200 nm and lengths ranging from 0.1 to 3.0 μm. Here, the rodlike structure of $MoTe_2$ is reported for the first time, and added to the list as one kind of new morphology of $MoTe_2$ nanomaterials. A mechanism for the formation of the nanorods is proposed. The sandwich-layered structure of Te–Mo–Te and the similarity in the structure between hexagonal α-$MoTe_2$ and hexagonal Te are responsible for the formation of nanorods of $MoTe_2$.

Introduction

The fabrication of nanorods has received increasing attention for their unique physical and chemical properties and a wide range of potential applications such as photonics[1,2] and nanoelectronics.[3] Considerable efforts have been placed on the synthesis of different kinds of nanorods/nanowires by many approaches, e.g., vapor−liquid−solid (VLS) growth,[4] the solution−liquid−solid (SLS) method,[5] the template-mediated growth method,[6] molten salt synthesis (MSS),[7,8] and others.

Semiconductor one-dimensional structures, i.e., nanotubes, nanorods, and nanowires, have stimulated intensive, worldwide research activities due to their interesting physical properties and corresponding potential applications in optoelectronic devices, solar energy conversion, nonlinear optics, photoelectrochemical cells, and heterogeneous photocatalysis.[9,10] α-$MoTe_2$ is a semiconductor with an indirect band gap of 1.0 eV and a direct optical band gap of 1.1 eV.[11] Since the optical band gap of α-$MoTe_2$ matches well with the solar spectrum, this material is used for electrodes in high-efficiency photoelectrochemical cells.[12] Despite the major importance of α-$MoTe_2$, to our knowledge, only the syntheses of $MoTe_2$ nanotubes fabricated by electron irradiation[13,14] and by the sonochemical method combined with heat treatment[15] have been reported. The synthesis of nanostructural $MoTe_2$ in other forms has not yet been reported. To date, though hundreds of papers reporting on the fabrication/synthesis of nanrods have been published, no report has been made on the synthesis of $MoTe_2$ nanorods. It seems that nanostructured tellurides such as $MoTe_2$ are more difficult

* Author to whom correspondence should be addressed. E-mail: gedanken@mail.biu.ac.il.
† Bar-Ilan University.
‡ China Academy of Engineering Physics.

(1) Snoke, D. *Science* **1996**, *273*, 1351−1352.
(2) Nakamura, S. *Science* **1998**, *281*, 956−961.
(3) Mirkin, C. A. *Science* **1999**, *286*, 2095−2096.
(4) Morales, A. M.; Lieber, C. M. *Science* **1998**, *279*, 208−211.
(5) Trentler, T. J.; Hickman, K. M.; Geol, S. C.; Viano, A. M.; Gibbons, P. C.; Buhro, W. E. *Science* **1999**, *270*, 1791−1994.
(6) Dai, H.; Wong, E. W.; Yu, Y. Z.; Fan, S. S.; Lieber, C. M. *Nature* **1995**, *375*, 769−772.
(7) Yoon, K. H.; Cho, Y. S.; Kang, D. H. *J. Mater. Sci.* **1998**, *33*, 2977−2984.
(8) Liu, Y.; Liu, Z.; Wang, G. *Appl. Phys. A* **2003**, *76*, 1117−1120.
(9) Hu, K.; Brust, M.; Bard, A. *Chem. Mater*. **1998**, *10*, 1160−1165.
(10) Murray, C. B.; Kagan, C. R.; Bawendi, M. G. *Science* **1995**, *270*, 1335−1338.
(11) Grant, A. J.; Griffiths, T. M.; Pitt, G. D.; Yoffe, A. D. *J. Phys. C* **1975**, *8*, L17−L23.
(12) Abruna, H. D.; Hope, G. A.; Bard, A. J. *J. Electrochem. Soc.* **1982**, *129*, 2224−2228.
(13) Galvan, D. H.; Rangel, R.; Adem, E. *Fullerene Sci. Technol.* **1999**, *7*, 421−426.
(14) Flores, E.; Tlahuice, A.; Adem, E.; Galvan, D. H. *Fullerene Sci. Techno.* **2001**, *9*, 9−16.
(15) Qiu, L. H.; Vilas, G. P.; Wei, Y.; Gedanken, A. *J. Mater. Chem.* **2003**, *13*, 2985−2988.

10.1021/ic049591a CCC: $27.50
Published on Web 08/12/2004

to prepare than the other chalcogenides such as $MoSe_2$ and MoS_2 nanorods. As we know, bulk α-$MoTe_2$ has a three-layered sandwich structure: one Mo hexagonal plane located between two hexagonal planes of Te.[16] It is known that one-dimensional nanostructures can be obtained from the rolling of natural or artificial lamellar structures. Under certain conditions, a layer structure may begin to curl (the interaction between the neighboring layers could be reduced from the edges of the layer, while keeping the interactions of the in-layer atoms or molecules), and the thus-obtained tubular structure may serve as the original driving force for the growth of one-dimensional nanostructures.[17,18] For example, layered σ-MnO_2 can serve as an important intermediate in the formation of MnO_2 nanorods.[19] Recently, we have found a route to synthesize the monoclinic β-$MoTe_2$ nanotubes. The β-polymorph was obtained when an amorphous $MoTe_2$ intermediate was calcined under a N_2 atmosphere. The intermediate amorphous $MoTe_2$ resulted from a sonochemical reaction of Te with $Mo(CO)_6$ in decalin. The β-$MoTe_2$ was formed in the shape of well-crystallized nanotubes.[15]

In this Article, we present the synthesis of α-$MoTe_2$ nanorods by annealing the $MoTe_2$ intermediate prepared by refluxing the mixture of $Mo(CO)_6$ and elemental tellurium in diphenylmethane. This route originates from our idea that the combination of the rolling-up mechanism for layered inorganic materials to form 1D nanostructures[17,18] with the molten salt synthesis mechanism[7,8] at high temperatures may work to result in α-$MoTe_2$ nanorods. The transmission electron microscopy (TEM) images of the intermediate show the as-prepared $MoTe_2$ is deposited in the amorphous phase on the unreacted Te particles. This structure of the $MoTe_2$ intermediate leads upon annealing to the formation of the α-$MoTe_2$ nanorods. In both of our cases of $MoTe_2$ nanotubes and nanorods, the difference between the routes mainly lies in the methods used to prepare the amorphous $MoTe_2$ intermediates. Interestingly, the morphologies of the as-heated products for the two cases are absolutely different from each other. So we also elucidate the formation mechanism.

Experimental Section

A typical preparation process is as follows: 50 mL of diphenylmethane (Aldrich, 99%), 528 mg of $Mo(CO)_6$ (Aldrich, 98%), and 512 mg of Te (Aldrich, 200 mesh, 99%) at a molar ratio of Mo:Te = 1:2 were sequentially added to a 50 mL round-bottom flask which was connected to a water-condensing system and an inert gas flowing system. The mixture was stirred with a magnetic stirring bar and heated at 145 °C in an oil bath for 20 h. The black precipitates were washed and separated by centrifugation with *n*-pentane four times, dried in a vacuum overnight, and annealed at 650 °C under N_2 for 4 h.

The phase composition and phase structure of the as-synthesized products were examined by X-ray diffraction (XRD), selected area electron diffraction (SAED), selected area energy dispersive spectroscopy (SAEDS) in combination with high-resolution transmission electron microscopy (HRTEM), energy dispersive X-ray (EDX) analysis, and X-ray photoelectron spectroscopy (XPS). XRD diffraction patterns were obtained by using a Bruker AXS D* Advance powder X-ray diffractometer (Cu Kα radiation, wavelength ~1.5406 Å), employing an operation potential of 40 kV and a current of 40 mA. SAED and SAEDS of one individual nanorod were conducted by using the related functions of a JEOL-2010 high-resolution transmission electron microscope. EDX data were measured by using a function attached to a scanning electron microscope, and XPS data were accumulated on an AXIS HS (Kratos analytical) electron spectrometer system with a monochromatized Al Kα standard X-ray source. The binding energies were calibrated by referencing the C 1s to 285.0 eV. The morphologies and micro- or nanostructure of the as-synthesized products were further characterized with a JSM-840 scanning electron microscope, a JEM-1200EX transmission electron microscope working at an accelerating voltage of 80 kV, and a JEOL-2010 high-resolution transmission electron microscope using an accelerating voltage of 200 kV. Samples for TEM and HRTEM were prepared by ultrasonically dispersing the products into absolute ethanol, then placing a drop of this suspension onto a copper grid coated with an amorphous carbon film, and then allowing the grid to dry in air.

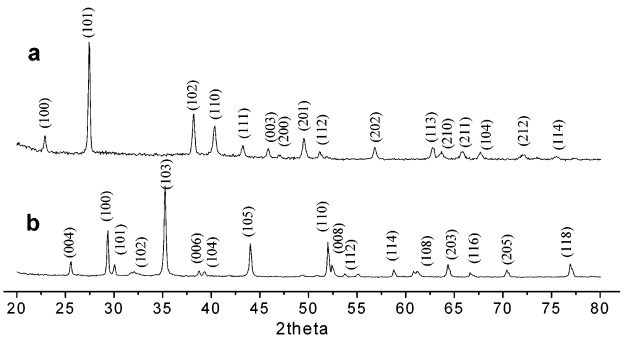

Figure 1. XRD patterns of (a) the initial $MoTe_2$ sample, only showing diffraction lines of Te, and (b) the corresponding annealed sample heated at 650 °C for 4 h under N_2.

Results and Discussion

XRD and EDX Studies. The XRD patterns of the as-prepared $MoTe_2$ product (assigned as the "initial $MoTe_2$ sample") and its annealed samples are presented in Figure 1. XRD results show that the initial $MoTe_2$ sample contains only crystals of unreacted tellurium (indexed to hexagonal Te with a space group of *P*3121 (152) corresponding to JCPDS 36-1452). And the XRD pattern of the annealed sample shows only peaks of the crystallized $MoTe_2$. All of the observed strong and sharp peaks can be readily indexed to hexagonal α-$MoTe_2$ (with lattice constants $a = 3.52$ Å, $b = 3.52$ Å, and $c = 13.97$ Å, compatible with the literature values of $a = 3.5182$ Å, $b = 3.5182$ Å, and $c = 13.9736$ Å (JCPDS 73-1650), with a space group of *P*63/*mmc* (194)). It will be argued that the initial $MoTe_2$ sample contains XRD amorphous $MoTe_2$ which crystallizes upon annealing (for 4 h at 650 °C) into an α-type structure. The unreacted crystalline tellurium whose diffraction peaks are observed in the XRD of the initial $MoTe_2$ sample disappeared

(16) Vollath, D.; Szabo, D. V. *Acta Mater.* **2000**, *48*, 953−967.
(17) Rothschild, A.; Popovitz-Biro, R.; Lourie, O.; Tenne, R. *J. Phys. Chem. B* **2000**, *104*, 8976−8981.
(18) Li, Y. D.; Li, X. L.; He, R. R.; Zhu, J.; Deng, Z. X. *J. Am. Chem. Soc.* **2002**, *124*, 1411−1416.
(19) Wang, X.; Li, Y. D. *Chem.—Eur. J.* **2003**, *9*, 300−306.

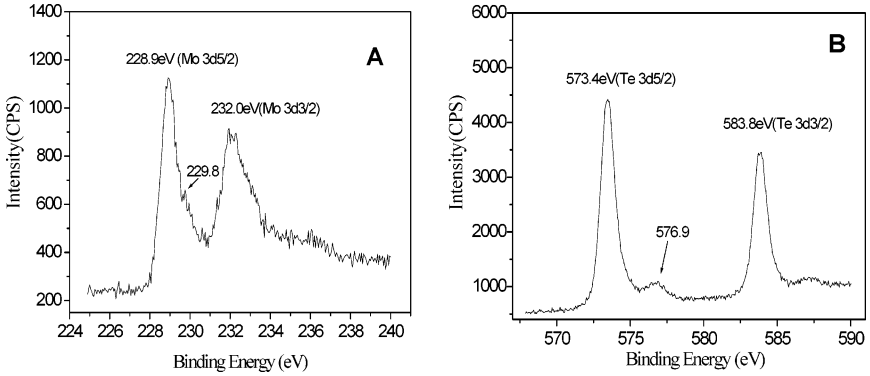

Figure 2. High-resolution XPS surveys in regions of Mo 3d (A) and Te 3d (B). Arrows indicate the possible existence of a slight trace of MoO_2 and tellurium oxide.

completely upon annealing. This is due to the low melting point of Te (450 °C), which has led to the vaporization of the excess of elemental Te during the heating process. Furthermore, we conducted the heat treatment at 650 °C for a shorter time of 2 h. But the XRD pattern (we do not list the corresponding XRD data here) shows coexistence of elemental hexagonal Te and α-$MoTe_2$ in the annealed sample. It indicates that the vaporization of elemental Te is quite slow or the transition of amorphous $MoTe_2$ into α-$MoTe_2$ needs a longer time than 2 h.

The elemental composition of Mo and Te in both the as-prepared and annealed samples was detected by EDX analysis. The detected molar ratios of Mo to Te are 23.3:69.5 (about 1:3) in the initial $MoTe_2$ sample and 28.7:59.0 (close to 1:2) in the annealed product. The initial $MoTe_2$ sample has a 49% excess of Te as compared with the initial reactant ratio of Mo:Te = 1:2. In other words, the loss of molybdenum is about 33% if it is assumed that all of the Te is present. Two possible explanations are offered for this loss: (1) the sublimation of $Mo(CO)_6$, which was carried away by the N_2 bubbling, and (2) the deposition of the in situ formed amorphous nanoparticles of $MoTe_2$ on the Te particles, which slows and even stops the reaction between $Mo(CO)_6$ and Te. Both explanations result in the existence of unreacted elemental Te crystals in the initial $MoTe_2$ sample.

XPS Studies. The binding energies and compositions of Mo and Te in the annealed $MoTe_2$ sample were further determined by XPS. Both photoelectrons of Mo 3d and Te 3d can be detected. High-resolution spectra of the annealed $MoTe_2$ in the core level regions of Mo 3d and Te 3d are shown in Figure 2. The observed binding energies are compared with the values measured over the years for the binding energies of Te 3d (573.5 eV for $3d^{5/2}$) in Te^{2-} compounds.[20] The same was done for the binding energies of Mo 3d (228.0 and 231.1 eV for $3d^{5/2}$ and $3d^{3/2}$, respectively). They were compared with those of Mo^{4+},[21] and with those of compounds such as MoO_x ($x = 2-3$) and MoS_2.[22,23] On the basis of this comparison the peaks at 228.9 and 232.0 eV in Figure 2A can be assigned to Mo 3d (for $3d^{5/2}$ and $3d^{3/2}$ peaks) of Mo^{4+} and those at 573.4 and 583.8 eV in Figure 2B to Te 3d (for $3d^{5/2}$ and $3d^{3/2}$)[23] of Te^{2-} in the compound $MoTe_2$. The observed chemical shifts of the binding energies of Mo $3d^{5/2}$ and Te $3d^{5/2}$ are −0.1 and 0.4 eV, respectively. XPS results further confirm the formation of $MoTe_2$. With a careful check of the Mo 3d and Te 3d core level regions of the annealed sample, we could detect very weak peaks at 229.8 eV in Figure 2A and at 576.9 eV in Figure 2B (labeled by arrows), which might be assigned to Mo 3d of MoO_2 (229.7 eV for Mo $3d^{5/2}$ [25]) and Te 3d of TeO_x (576.9 eV for $3d^{5/2}$ compared with literature values of 577.3 eV[26] and 576.6 eV[27]). In this case, XPS results indicate that the surface of the annealed $MoTe_2$ sample was slightly oxidized due to its air-sensitive properties and exposure to air. Similarly, tellurium oxide was observed for the tellurium in $Ni^{VI}Te_2$.[24] No other impurity peaks were observed in the annealed $MoTe_2$ sample. So the XPS and XRD analyses reveal that freshly synthesized samples of $MoTe_2$ nanorods should be pure within the limits of instrumental error.

Electron Microscopy Studies (TEM, SEM, HRTEM, SAEDS). The morphologies of the initial $MoTe_2$ sample were characterized by TEM and HRTEM. And typical images are shown in Figure 3. Figure 3a shows that the initial $MoTe_2$ sample contains agglomerated dark amorphous particles that are deposited onto brighter fields observed on the grid (indicated by a white arrow). By contrast, the brightest fields labeled by a black arrow correspond to the carbon-coated grid itself. The dark fields reveal particles with a wide distribution of sizes ranging from 50 to 200 nm. One typical HRTEM image of an individual amorphous particle is shown in Figure 3b. The image shows that on part of the seed clear fringes arranged in two directions (indicated by I and II in Figure 3b) are clearly observed. And the fringe spacings are 0.238 and 0.319 nm, respectively. This is consistent with the *d* values 0.2349 and 0.3233 nm of crystal planes (102)

(20) Ricco, A. J.; White, H. S.; Wrighton, M. S. *J. Vac. Sci. Technol., A* **1984**, *2*, 910−915.
(21) Wu, H. M.; Chen, S. A. *Synth. Met.* **1988**, *26*, 225−236.
(22) Brox, B.; Olefjord, I. *Surf. Interface Anal.* **1988**, *13*, 3−6.
(23) Cizaire, L.; Vacher, B.; Mogne, T. L.; Martin, J. M.; Rapoport, L.; Margolin, A.; Tenne, R. *Surf. Coat. Technol.* **2002**, *160*, 282−287.
(24) Rotlevi, O.; Dobson, D. K.; Rose, D.; Hodes, G. *Thin Solid Films* **2001**, *387*, 155−157.
(25) Patterson, T. A.; Carver, J. C.; Leyden, D. E.; Hercules, D. M. *J. Phys. Chem.* **1976**, *80*, 1702−1708.
(26) Bahl, M. K.; Watson, R. L.; Irgolic, K. J. *J. Chem. Phys.* **1977**, *66*, 5526−5535.
(27) Swartz, W. E.; Wynne, K. J.; Hercules, D. M. *Anal. Chem.* **1971**, *43*, 1884.

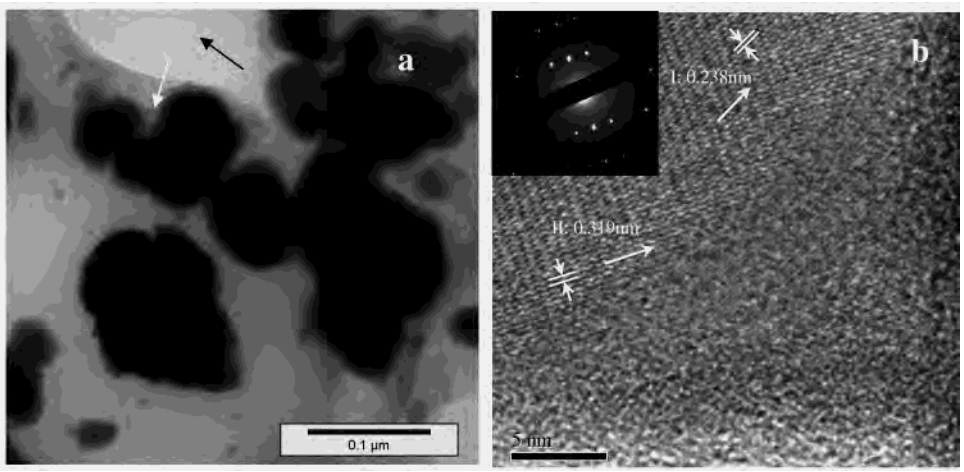

Figure 3. Morphologies of the initial $MoTe_2$ intermediate. (a) A typical TEM image. Black and white arrows indicate the unoccupied places of the grid and the thus-formed amorphous $MoTe_2$, respectively. By contrast, the dark particles are the unreacted Te. (b) An HRTEM image. The inset is a SAED pattern taken on the zone of Te seed. The fringes arranged in two directions, I and II, have spacing values of 0.238 and 0.319 nm, corresponding to the interplane distances of (102) and (011) of hexagonal Te, respectively. $MoTe_2$ is in the amorphous state.

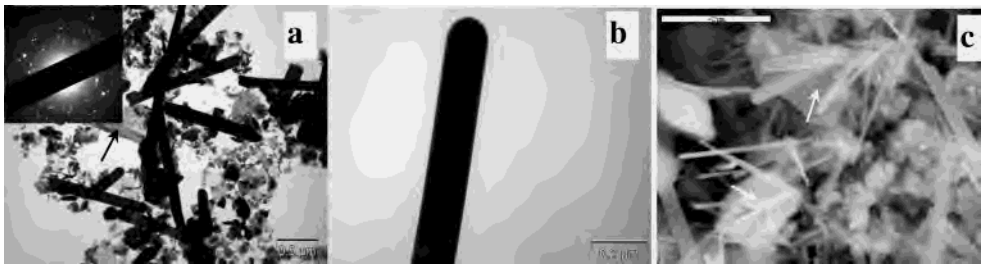

Figure 4. Morphologies of the sample observed by TEM and SEM. The sample was annealed under N_2 at 650 °C for 4 h. (a) A TEM image of the assembly (the inset is the corresponding ED pattern). The scale bar is 500 nm. (b) A TEM image observed at higher magnification of a randomly selected individual $MoTe_2$ nanorod. (c) An SEM image (arrows indicating sheets and flakes).

and (011) of the hexagonal Te (corresponding to JCPDS 36-1452). The individual particle was further tested by SAED and SAEDS. The SAED pattern, shown in the inset of Figure 3b, was taken on the seed zone. The spotted pattern corresponds to the hexagonal Te (JCPDS 36-1452). SAEDS tests were carried out with an electron beam size of 15 nm, and the results show that the elemental compositions of the seed and other parts of individual particles are quite different. The percentage of Te on the seed is almost 3 times higher than that of other amorphous parts. So we assign these seeds/cores to the unreacted Te particles. These particles function according to our explanation as seeds or cores randomly located inside the aggregated amorphous $MoTe_2$. SAEDS also shows that the corresponding amorphous parts are composed of Mo and Te at molar ratios close to 1:2. Their formation in the initial $MoTe_2$ sample is in agreement with our explanation of the XRD results; i.e., initial elemental Te particles were consumed by the reaction

$$Mo(CO)_6 + 2Te \rightarrow MoTe_2 + 6CO \qquad (1)$$

and formed into insoluble amorphous $MoTe_2$. The $MoTe_2$ is deposited on the unreacted Te particles, and this slows the reaction and results in Te-seeded amorphous $MoTe_2$ particles.

The morphologies of the corresponding annealed sample were characterized by SEM and TEM and are shown in Figure 4. Figure 4a is a typical TEM image of the products annealed at 650 °C under N_2 for 4 h. This image clearly indicates the coexistence of rods and sheets and other irregular nanoparticles of $MoTe_2$. A significant portion (about ~50%) in volume of the sample dispersed on the TEM grids shows rodlike structures. The observed nanorods have a wide dimensional distribution of diameters, 50−200 nm, and lengths ranging from 0.1 to 3 μm. It is worth noting that each of the observed nanorods has one end which is well-developed into coronary shapes while the other end is irregularly shaped. The reason is not so clear now but might be related to the formation mechanism. Figure 4b shows an individual $MoTe_2$ nanorod observed at a higher magnification. The observed end of this nanorod is well-shaped and uniformly/gradually constructed with the main body. The SEM image (Figure 4c) shows morphological and dimensional results similar to those observed by TEM. But in the SEM image bigger sheets are more clearly observed (indicated by arrows). The ED pattern of the annealed sample (the inset in Figure 4a) is a mixture of spotted and diffused cycles, which imply the sample contains polycrystals and nanosized particles. Further annealing experiments were also conducted by lengthening the heating time to 10 h, and the annealed product's morphologies revealed by TEM are very similar to those of the sample annealed for 4 h.

The morphologies and crystallization of the annealed products were further investigated by HRTEM. Figure 5 shows the SAED patterns and lattice fringes of two randomly

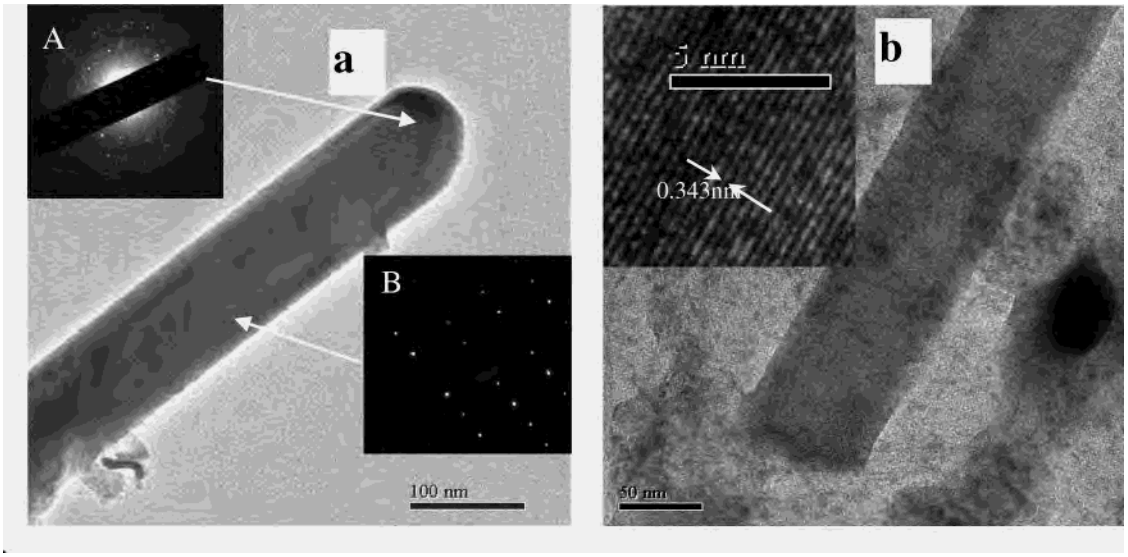

Figure 5. Individual $MoTe_2$ nanorods tested with HRTEM. (a) A selected nanorod and its SAED patterns (insets A and B tested on the end and in the middle of the rod, respectively). (b) Lattice fringes detected on an individual rod.

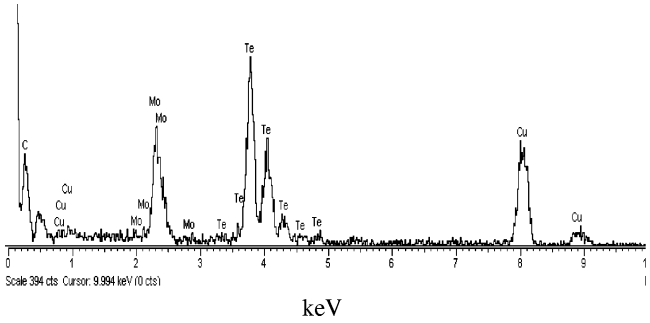

Figure 6. SAEDX analysis of an individual nanorod.

selected individual nanorods of the product annealed at 650 °C for 4 h. The SAED patterns, shown in insets A and B in Figure 5a, were detected on the end and in the middle of the nanorod observed, respectively. The patterns reveal that the nanorod is well-crystallized in the middle while less crystallized on the end. Figure 5b shows another individual $MoTe_2$ nanorod and its lattice fringes with interplane spacing of 0.343 nm (measured and indicated in the inset), which corresponds to the (004) plane (with spacing of 0.349 nm) of hexagonal α-$MoTe_2$. It is necessary to point out that, searching carefully throughout other areas of the sample, we were not able to locate either onion-like structures or fullerene nanoparticles, as they are usually found in WS_2 or MoS_2.[16]

SAEDS was taken on an individual nanorod, and the pattern is shown in Figure 6. The results exhibit the existence of Mo and Te with a molar ratio of 1.0:1.9, in good agreement with EDX results and close to the stoichiometric ratio 1:2 of $MoTe_2$. Peaks of copper and carbon (the leftmost unlabeled peaks) are raised from the TEM grid itself. It also shows 16 atom % oxygen in the annealed sample due to the slight oxidization of $MoTe_2$ during its exposure to air. The slight oxidization of the sample is also confirmed by XPS results (shown in Figure 2).

Formation Mechanism of the Nanorods. On the basis of the above-obtained data, we can rule out the VLS or SLS method as a possible mechanism for the formation of the $MoTe_2$ nanorods. If one of these mechanisms would operate for the nanorod formation, the SAEDX would show an increased concentration of Te at the end of the rod. In our case, there are no spherical liquid droplets of Mo or Te at the tips of the $MoTe_2$ nanorods, which is required evidence for the VLS[4,28] and/or SLS[5] mechanisms. Xia and the co-workers have elucidated that the anisotropic crystalline structures of elemental Se and Te may lead to the formation of 1D nanostructures of nanorods or nanotubes due to the Ostward ripening of Se or Te nanoparticles formed in situ in a solution.[29] In our case, the annealing temperatures are high, up to 650 °C, and the elemental Te will melt at about 450 °C. So we can rule out this mechanism for the formation of $MoTe_2$ nanorods.

As we have previously demonstrated in Figure 4, the morphologies of the annealed $MoTe_2$ sample are typically rolling sheets and nanorods and each rod has only one spherical end smoothly connected to the main body. It is known that layered materials can form into one-dimension (1D) nanostructures by the rolling-up mechanism.[17,18,30] Under certain conditions, for example, heating at high temperatures, a layer structure may begin to curl, and the thus-obtained tubular structure may serve as the original driving force for the growth of 1D nanostructures.[19] We know that α-$MoTe_2$ (hexagonal type) has a sandwich-layered structure,[16] which is indispensable in the rolling mechanism. In our case, we believe that the $MoTe_2$ nanorods were formed by a mechanism similar to the rolling-up mechanism but with the assistance of the molten Te during the annealing process. We propose the nanorod formation process has the following steps.

(1) The elemental Te inside the Te-seeded amorphous $MoTe_2$ particles (shown in Figure 3) melts at increased

(28) Wagner, R. S.; Ellis, W. C. *Appl. Phys. Lett.* **1964**, *4* (5), 89.
(29) Xia, Y. N.; Yang, P. D.; Sun, Y. G.; Wu, Y. Y.; Mayers, B.; Gates, B. Yin, Y. D.; Kim, F.; Yan, Y. Q. *Adv. Mater. 15* (5), 353−389.
(30) Li, W. Z.; Xie, S. S.; Liu, W.; Zhao, R.; Zhang, Y.; Zhou, W. Y.; Wang, G.; Qian, L. X.; Liu, W. *J. Mater. Sci.* **1999**, *34*, 2745−2749.

temperatures (the mp of Te is about 450 °C), and the liquid droplets of Te in an individual $MoTe_2$ particle aggregate due to the tendency to lower its energy.

(2) Amorphous $MoTe_2$ begins to crystallize when the temperatures are high enough and reach its critical crystalline temperatures and forms into layered structures which tend to roll up with further heating. So liquid droplets of Te inside the rolling particles are shaped into cylinders along the axis of the tubular structures and may penetrate radially and go between the rolling layers. The liquid droplet, which is smaller than the $MoTe_2$ particle, may not be located in the center of the $MoTe_2$ particle due to the initial irregular shape of the $MoTe_2$ particles. Liquid Te will be dispersed non-uniformly in each $MoTe_2$ tubular structure.

(3) Owing to the similar hexagonal layered structures and having elemental Te in common, the molten Te serves as the flux to $MoTe_2$ and helps the growth of crystalline $MoTe_2$ into rods.

The third step is essential to the conversion of α-$MoTe_2$ into nanorods. This step is similar to the molten salt synthesis mechanism in that the molten salt acting as the flux helps the crystallization and the development of morphologies of nanorods.[7,31] On one hand, the $MoTe_2$ tubular structures continue to tighten toward the axis due to the rolling forces, and the rolling process is accelerated and maximized due to the wetting of α-$MoTe_2$ with liquid Te. (We must point out that this might be the key reason we failed to obtain monoclinic β-$MoTe_2$ in the shapes of nanorods but nanotubes in another syntheses.) Meanwhile, the replacement of Te atoms in $MoTe_2$ with those from liquid Te might take place ($2Te^* + MoTe_2 \rightarrow MoTe^*_2 + 2Te$). The above two factors might help the encapsulated liquid Te to migrate along the rolled structures and yield solid 1D nanostructures. On the other hand, the molten Te on the outer surfaces is lost due to its vaporization. During this process, the tubular structure might be blocked on one end. We believe that it is impossible for both ends to be blocked because at least one end should give space for the squeezed liquid Te inside. And the liquid Te continues to assist the growth of crystallized α-$MoTe_2$ rods along the axis till it becomes completely dry. This way nanorods with one well-developed end are always observed.

The exact formation mechanism of the morphologies of the crystallized α-$MoTe_2$ nanorods still remains obscure, and further investigation is undoubtedly needed.

It should be pointed out that, in a similar annealing process employed on an amorphous intermediate that was conducted sonochemically, we have obtained nanotubes of $MoTe_2$, and the telluride was formed into the β-phase.[15] This difference is accounted for in the following way: the sonochemically prepared $MoTe_2$ particles might contain nanocrystals of β-phase $MoTe_2$, which is high-temperature stable phase, formed in the extremely high temperature sonochemical process. The β-nanocrystals play the role of seeds in crystallization, and the $MoTe_2$ was crystallized into the β-phase. During the annealing process, the formation of the 1D nanostructures of β-$MoTe_2$ is also governed by the rolling-up mechanism. However, compared with our present case in which α-$MoTe_2$ has hexagonal structure similar to that of α-Te and the Te seeds help the formation of nanorods through the mechanism as we have explained above, β-$MoTe_2$ is monoclinic and has quite a difference in structures with the encapsulated seeds of hexagonal α-type Te. In the case of β-$MoTe_2$, Te seeds do not tend to serve as the flux to the crystallization of β-type $MoTe_2$. So, both lead to different formation mechanisms which result in nanotubes in the β-phase case and nanorods in α-$MoTe_2$. Our supposed mechanism helps to explain both quite different results.

(31) Wang, W. Z.; Xu, C. K.; Wang, X. S.; Liu, Y. K.; Zhan, Y. J.; Zheng, C. L.; Song F. Q.; Wang, G. H. *J. Mater. Chem.* **2002**, *12*, 1922−1925.

Conclusions

In summary, we have demonstrated a simple method for the synthesis of $MoTe_2$ nanorods via annealing amorphous $MoTe_2$ particles prepared by a solution route. We obtained $MoTe_2$ nanorods with diameters of 50−200 nm and lengths ranging from 0.1 to 3 μm. The as-prepared $MoTe_2$ particles contain unreacted smaller Te particles, which act as the irregular seeds. The Te seeds play a key role in the formation of the $MoTe_2$ nanorods during annealing at 650 °C in a nitrogen atmosphere. Due to the similarity of their hexagonal layered structures, the α-$MoTe_2$ particles tend to form into sheets and then roll up into tubular structures. More importantly, the molten Te, acting as the wetting flux for the rolling $MoTe_2$ layers, assists the growth of the in situ formed tubular structures into nanorods. To the best of our knowledge this is the first time that the synthesis and characterization of $MoTe_2$ nanorods has been reported. Although our present efforts have mainly emphasized α-$MoTe_2$ nanorods, we believe that this route might be modified and possibly extended to other layered inorganic materials.

Acknowledgment. L.H.Q. is grateful for a Fred and Barbara Kort Sino-Israel postdoctoral fellowship and to the China Scholarship Council for its kind support. He also thanks Dr. Tova Tamari, Dr. Judith Grinblatt, Dr. Elea Sominski, and Dr. Yossi Gofer for their help with TEM, HRTEM, SEM, and XPS measurements and Dr. Yuri Koltypin for his technical support in the laboratory.

IC049591A